Published online 9 January 2018

Nucleic Acids Research, 2018, Vol. 46, No. 6 ***3187–3197***
doi: 10.1093/nar/gkx1316

Viral suppressors of RNAi employ a rapid screening mode to discriminate viral RNA from cellular small RNA

Mohamed Fareh[1], Jasper van Lopik[1], Iason Katechis[1], Alfred W. Bronkhorst[2], Anna C. Haagsma[1], Ronald P. van Rij[2,*] and Chirlmin Joo[1,*]

[1]Kavli Institute of NanoScience and Department of BioNanoScience, Delft University of Technology, Delft 2629 HZ, The Netherlands and [2]Department of Medical Microbiology, Radboud University Medical Center, Radboud Institute for Molecular Life Sciences, Nijmegen 6525 GA, The Netherlands

Received September 6, 2017; Revised December 21, 2017; Editorial Decision December 26, 2017; Accepted January 03, 2018

ABSTRACT

RNA interference (RNAi) is an indispensable mechanism for antiviral defense in insects, including mosquitoes that transmit human diseases. To escape this antiviral defense system, viruses encode suppressors of RNAi that prevent elimination of viral RNAs, and thus ensure efficient virus accumulation. Although the first animal Viral Suppressor of RNAi (VSR) was identified more than a decade ago, the molecular basis of RNAi suppression by these viral proteins remains unclear. Here, we developed a single-molecule fluorescence assay to investigate how VSRs inhibit the recognition of viral RNAs by Dcr-2, a key endoribonuclease enzyme in the RNAi pathway. Using VSRs from three insect RNA viruses (Culex Y virus, Drosophila X virus and Drosophila C virus), we reveal bimodal physical interactions between RNA molecules and VSRs. During initial interactions, these VSRs rapidly discriminate short RNA substrates from long dsRNA. VSRs engage nearly irreversible binding with long dsRNAs, thereby shielding it from recognition by Dcr-2. We propose that the length-dependent switch from rapid screening to irreversible binding reflects the main mechanism by which VSRs distinguish viral dsRNA from cellular RNA species such as microRNAs.

INTRODUCTION

All living organisms are constantly exposed to molecular parasites including viruses. Antiviral immune responses have evolved to eliminate these invaders, ensuring survival of host organisms. Insects, including mosquitoes that transmit human diseases such as dengue and Zika fever, rely on the RNA interference (RNAi) pathway to fight viruses (1). In the RNAi pathway, the endoribonuclease Dicer-2 (Dcr-2) complexed with RNA-binding protein partners cleave viral double-stranded (ds) RNAs into ∼21-nt viral small interfering RNAs (vsiRNAs) (2–4). Dicer proteins preferentially select dsRNA substrates with 2-nt 3′ overhang using the PAZ domain. However, *Drosophila melanogaster* Dcr-2 appears to have an alternative substrate recognition mode to process viral dsRNA in a PAZ-independent manner, which allows for cleaving dsRNA with a blunt end (5). This non-conventional substrate recognition is coupled with adenosine triphosphate (ATP) hydrolysis and structural rearrangement of the helicase domain (6). Upon viral dsRNA recognition and cleavage by Dcr-2, the vsiRNAs are loaded into Argonaute-2 to guide the effector nuclease complex called RISC (RNA Induced Silencing Complex) to target RNAs. VsiRNA-loaded RISC then cleaves viral single-stranded RNA molecules that have escaped Dcr-2 (4). Specificity of target search is conferred by base pairing between guide RNAs embedded within RISC and target RNAs (7–9). The antiviral activity of RNAi is evident from the observation that genetic inactivation of the RNAi pathway promotes the proliferation of the invading viruses to the detriment of the insect host (10–13).

As a counter-defense, viruses evolved a multitude of proteins called Viral Suppressors of RNA silencing (VSRs) that antagonize the RNAi pathway (11,14–17). The antiviral RNAi response is activated by the detection of intracellular double-stranded RNAs (dsRNA) that are essential intermediates in replication of RNA viruses, or may be produced by convergent transcription from both strands of dsDNA viruses (2,18). This initial stage of the antiviral RNAi response would be an effective target for viral interference. Indeed, many VSRs possess dsRNA binding motifs that recognize viral RNA molecules to protect them from

*To whom correspondence should be addressed. Tel: +31 152 783 220; Fax: +31 152 781 202; Email: c.joo@tudelft.nl
Correspondence may also be addressed to Ronald van Rij. Tel: +31 243 617 574; Email: Ronald.vanRij@radboudumc.nl
Present Address: Alfred W. Bronkhorst, Institute of Molecular Biology, D-55128 Mainz, Germany.

Dcr-2 cleavage and/or prevent loading of vsiRNAs into Argonaute (2,11,14,19–21). Yet, alternative modes of RNAi suppression exist. For example, several VSRs physically interact with RNAi protein effectors via protein-protein interactions and alter the ability to cleave viral RNAs (16,22–24). Although the interplay between viral RNAs, VSRs, and RNAi machinery has been investigated, the molecular mechanisms by which VSRs discriminate viral dsRNA from other cellular RNA species remain largely unknown.

Recent single-molecule approaches allow for real-time observation of macromolecular complexes in action with high spatiotemporal resolution (25–28). Here we developed single-molecule assays to visualize in real-time RNA recognition by VSRs from three insect RNA viruses, Culex Y virus (CYV) VP3, Drosophila X virus (DXV) VP3 and Drosophila C virus (DCV) 1A (20). Our single-molecule data indicate that these VSRs engage physical interactions with the viral RNA molecules, which prevents RNA recognition by Dcr-2. VSRs use a rapid screening mode to distinguish viral RNA substrates from host RNAs such as precursor or mature duplex microRNAs. The length of the double-stranded region is the most critical feature for selection. Short dsRNA molecules are rapidly rejected after initial contact with the VSRs, whereas long dsRNA molecules achieve irreversible binding that preclude Dcr-2 recognition. We propose that VSRs rely on the length of the stem region to discriminate viral RNAs from other structured cellular RNA species.

MATERIALS AND METHODS

Protein purification

GST-Loqs-PD was expressed in *Escherichia coli* BL21 DE3 strain. When the bacterial cultures had reached an OD_{600} of 0.8, protein expression was induced with 0.1 mM isopropyl-ß-D-1-thiogalactopyranoside (IPTG). Following overnight incubation at 16°C, the cells were resuspended in lysis buffer containing 10 mM Tris–HCl (pH 8), 150 mM NaCl, 1 mM ethylenediaminetetraacetic acid (EDTA), 7 mM dithiothreitol (DTT), 100 μg/ml lysozyme and 2% Sarkosyl (w/v). Cells were lysed by sonication (SONICS, VC130) for 1 min (40% amplitude, 1 s pulse, 2 s break) on ice. After sonication, the cell debris was collected by centrifugation at 12 000 rpm for 10 min. To concentrate the protein, the supernatant was transferred into an AMICON Ultra-15 Centrifugal filter device. A total of 20 mM CHAPS and 2% Triton-X100 were then added to the concentrated protein and the solution was incubated for 30 min at 4°C. Following this, 1 ml of GST-beads (Glutathione Sepharose 4B) were added to the solution with an incubation time of 1 h at 4°C. To purify the protein, the solution was applied to a GST-Gravi-Trap column. After applying the sample, the column was washed with 20 ml of 2% Triton-LqPD-buffer [10 mM Tris–HCl (pH 8), 150 mM NaCl, 1 mM EDTA, 2% Triton-X100] and 20 ml of LqPD-buffer [10 mM Tris–HCl (pH 8), 150 mM NaCl, 1 mM EDTA]. The GST-fusion protein was eluted by applying 10 ml of 10 mM Glutathione (in LqPD-buffer) to the column. The eluted protein was collected in 1 ml fractions and stored at −80°C in buffer containing 10 mM Tris–HCl (pH 8), 150 mM NaCl, 1 mM EDTA and 15% glycerol. The concentration of the samples was determined by measuring the absorption at 280 nm wavelength using spectrophotometer. Sodium dodecyl sulphate-polyacrylamide gel electrophoresis (SDS-PAGE) gel and western-blot analysis confirmed the purity of the protein.

CYV-VP3, DXV-VP3 and DCV-1A were expressed as MBP fusion proteins as previously described (20). Briefly, the CYV-VP3, DXV-VP3 and DCV-1A coding sequences were cloned downstream of the MBP coding sequence in the multiple cloning site of pMAL-c2X (New England Biolabs) using the EcoRI and SalI restriction sites for DCV-1A and BamHI and HindIII sites for CYV and DXV-VP3. As a consequence, the MBP sequence and the viral sequences are separated by a linker of 24 (DCV-1A) and 26 amino acids (CYV and DXV-VP3). The plasmids were transformed into *E. coli* BL21 (DE3). When the bacterial cultures reached an OD_{600} of 1.2, protein expression was induced by the addition of 1 mM of IPTG. Following overnight incubation at 18°C, the recombinant proteins were affinity-purified on amylose resin columns according to the manufacturer's instructions (New England Biolabs). The proteins were dialyzed to buffer (20 mM Tris–HCl, 0.5 mM EDTA, 5 mM $MgCl_2$, 1 mM DTT, 140 mM NaCl, 2.7 mM KCl) and stored in dialysis buffer containing 30% glycerol, as described previously (20). Protein concentrations were determined with the Bio-Rad (Bradford) Protein Assay.

AP-TEV-6xHis tagged Dcr-2 protein was cloned, expressed and purified by GenScript (NJ, USA) using a published protocol (29). In short, proteins were expressed from insect cells (Sf9 cell line) using the Bac-to-Bac Baculovirus expression system F1 and were purified using Ni-NTA beads (QIAGEN). The protein was incubated with *Tobacco Etch Virus* (TEV) protease to cleave off the His-tag, purified by agarose SP Sepharose and Superdex 200, and dialyzed in Dcr-2-buffer (10 mM HEPES, 150 mM NaCl, 5% Glycerol, 1 mM TCEP, pH 7.4) (Figure 1A). The BirA enzyme was simultaneously expressed with Dcr-2 in Sf9 cells, which promoted ∼100% *in vivo* biotinylation of the AP-tag in the N-terminus of Dcr-2 (Figure 1B), when the media was supplemented with 1 mg/ml of free biotin as described elsewhere (30,31).

Dicer processing

Dcr-2 cleavage reactions were performed at 25°C in a total volume of 20 μl, in 25 mM Tris (pH 8.0), 100 mM KCl, 10 mM $MgCl_2$, 1 mM TCEP, 5 mM ATP, 2.5 nM of internally Cy5-labeled dsRNA, 100 nM of Dcr-2 and 100 nM of the purified LqPD. Dcr-2 and LqPD were pre-incubated together during 5 min to promote protein complex assembly. The cleavage reactions were started by adding 100 nM of Dcr-2–LqPD and stopped with two volumes of 2 × formamide loading buffer (95% formamide, 18 mM EDTA, 0.025% SDS, xylene cyanol, bromophenol blue) as described elsewhere (5). The RNA samples were separated on 10% urea polyacrylamide gel and scanned with a Typhoon imager (GE Healthcare).

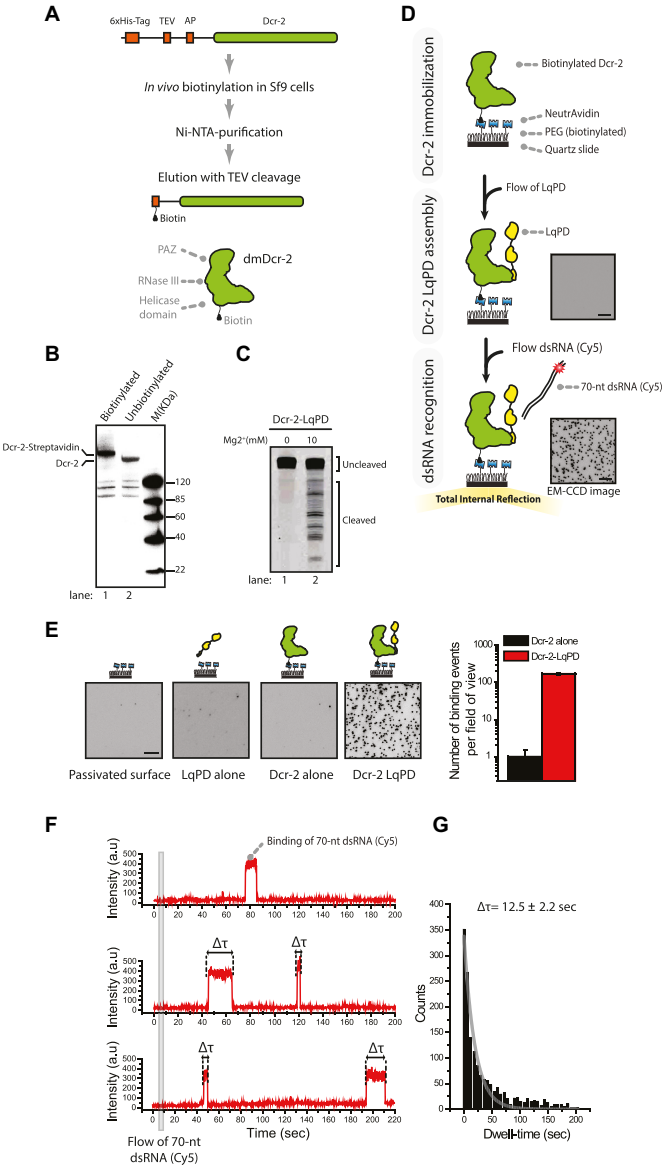

Figure 1. Development of a single-molecule assay for real-time observation of viral RNAs recognition by Dcr-2 complex. (**A**) Schematic representation of sample preparation. Dcr-2 was constructed with 6xHis, TEV and AP tags which were used for Ni-NTA purification, elution, and *in vivo* biotinylation, respectively. Dcr-2 proteins were biotinylated in Sf9 cells. The protein was purified using Ni-NTA column and eluted by 6xHis-tag cleavage by the TEV protease. (**B**) Western blot analysis displays the efficiency of *in vivo* biotinylation of AP-tagged Dcr-2 in the presence (lane 1) or absence (lane 2) of 1 mg/mL free biotin in the culture medium. The biotinylated Dcr-2 bound to StreptAvidin, which resulted in the shift observed in lane 1. (**C**) *In vitro* cleavage assay of Cy5-labeled 70-nt dsRNA with blunt end by Dcr-2–LqPD in the absence (lane 1) and presence (lane 2) of 10 mM $MgCl_2$. The top band indicates non-cleaved dsRNA, and the lower bands indicate cleavage products. (**D**) Schematic representation of single-molecule immobilization. Dcr-2 was conjugated to a polymer-coated surface via NeutrAvidin-biotin interaction. Contaminant proteins were washed away before the introduction of LqPD recombinant protein into the imaging chamber. Dcr-2 and LqPD were incubated together for 5 min to promote protein–protein interaction on the surface of the imaging chamber. Non-bound LqPD was washed away before Cy5-labeled 70-nt dsRNA was introduced. Interactions between the surface-immobilized Dcr-2 complexes with Cy5-labeled dsRNA were visualized through TIRF microscopy. Dots in the EM-CCD image reflect docking of dsRNA to individual Dcr-2–LqPD complexes. The EM-CCD image illustrated the binding events over 25 × 25 μm field of view. Scale bar, 5 μm. (**E**) EM-CCD images illustrating stable docking of Cy5-labeled dsRNA to passivated surface without any protein (left), passivated surface with LqPD non-specifically immobilized (second image), surface immobilized Dcr-2 in the absence of LqPD (third image) and surface immobilized Dcr-2–LqPD complexes. Scale bar, 5 μm. The histogram (right panel) compares the absolute binding activity of Dcr-2 alone and Dcr-2–LqPD complex. Data are presented as averages and SD of three independent experiments. In each experiment snapshots from 10 fields of view were analyzed. (**F**) Representative time traces (at a time resolution of 300 ms) exhibiting recognition of multiple Cy5-labeled 70-nt dsRNA by a single Dcr-2–LqPD complex. The dwell-time ($\Delta\tau$) is the time between docking and dissociation. The 70-nt Cy5-dsRNA was added at a time period of 5 s. (**G**) Dwell-time histogram derived from binding events recorded for 450 s in a pre-steady state condition. The distribution was fitted with a single exponential decay (gray line) where the average dwell-time is $\Delta\tau = 12.5 \pm 2.2$ s. Data are presented as average and SD of three independent experiments.

RNA preparation and labeling

All RNA constructs used in this study were synthesized by ST-Pharm, IBA-Lifesciences and ELLA Biotech. RNA hairpins were generated by ligation of two synthetic RNAs (Supplementary Table S1). First, a single stranded RNA containing 5′ phosphate (acceptor, 200 pmol) was mixed with the other strand containing 3′OH (donor, 100 pmol) in TE buffer containing 100 mM NaCl. This mixture (20 μl) was subsequently annealed by heating to 80°C followed by slowly cooling in a thermal cycler (−1°C/4 min). The annealed substrate was ligated with 3 μl T4 RNA ligase (Ambion, 5 U/μl), 3 μl 0.1% bovine serum albumin, 5 μl 10× ligation buffer provided and 19 μl H_2O at 16°C for 24 h. After ethanol precipitation, the RNA was purified from a 12.5% urea polyacrylamide gel (32). The RNA strands were labeled with the NHS-ester form of Cy dyes (GE Healthcare) at nearly 100% efficiency without compromising their structure and the processing by RNA binding proteins (31). In case of short siRNA that does not contain any loop structure (Figure 4), sense strand was labeled with Cy3 and annealed to an antisense strand labeled with Cy5 to ensure exclusive analysis of double-stranded RNA population. For simplicity, we show only Cy5 fluorescence signal in the time traces.

Microfluidic chamber

To eliminate non-specific surface adsorption of proteins and nucleic acids, the quartz surface (Finkenbeiner) of the microfluidic chamber was coated with poly-ethyleneglycol (mPEG-Succinimidyl Valerate, MW 5000, Laysan). A subpopulation of the PEG (∼2.5%) had biotin at the end (Biotin-PEG-SVA, MW 5000, Laysan). NeutrAvidin was layered on the surface via conjugation with the biotin. The details can be found elsewhere (33). Finally, biotinylated Dicer IPs were specifically immobilized via the biotin-NeutrAvidin interaction. The binding between biotinylated Dicer and NeutrAvidin is stable for several hours without any noticeable dissociation.

Single-molecule observation of Dicer–RNA interaction

Fifty microliters of NeutrAvidin (100 μg/ml, Invitrogen) was incubated for 2 min in the chamber. After washing un-

bound NeutrAvidin away with 100 μl T50 buffer (10 mM Tris–HCl pH 8, 50 mM NaCl), 50 nM biotinylated Dcr-2 (20 μl) was incubated for 5 min in the chamber. After washing the unbound proteins away with 100 μl Dcr-2-buffer (25 mM Tris pH 8.0, 100 mM KCl, 10 mM $MgCl_2$ and 1 mM TCEP,), 50 nM of recombinant LqPD was introduced into the imaging chamber and incubated with surface immobilized Dcr-2 for 5 min. After washing away the unbound LqPD with Dcr-2-buffer, 100 pM dye-labeled dsRNA was injected in the imaging buffer. As a negative control, LqPD alone (50 nM) lacking Dcr-2 was pre-incubated for 5 min in the passivated chamber. Unbound proteins were washed away with 100 μl of Dcr-2-buffer, before the introduction of 100 pM dye-labeled dsRNA.

The imaging buffer consisted of 25 mM Tris [pH 8.0], 100 mM KCl, 10 mM $MgCl_2$, 1 mM TCEP, an oxygen scavenging system (0.8% glucose (v/v), 0.1 mg/ml glucose oxidase (Sigma-Aldrich), 17 μg/μl catalase (Roche)) to reduce photobleaching and 1 mM Trolox (Sigma-Aldrich) to reduce photoblinking of the dyes (34).

Single-molecule observation of VSR–RNA interaction

VSR proteins were immobilized on the surface of the microfluidic chamber using a biotinylated anti-MBP antibody (US Biological Sciences, M2155–09P). A total of 66 nM of biotinylated anti-MBP antibody was incubated with the NeutrAvidin coated-surface for 2 min. The unbound antibodies were washed away with 100 μl of T50 buffer before the introduction of 1–100 nM VSRs proteins. The unbound proteins were washed away with imaging buffer, followed by the introduction of 100–200 pM dye-labeled dsRNA in imaging buffer.

Single-molecule data acquisition

The fluorescent label Cy3 was imaged using prism-type total internal reflection microscopy at an excitation at 532 nm (Compass 215M-50, Coherent). Cy5 was excited by a 633 nm solid-state laser (CVI Melles Griot 25 LHP 928, 633 nm). When obtaining the time traces, the Cy3 and Cy5 molecules were excited with 532 nm and 633 nm laser light sources as weakly as possible (4–5 mW) to minimize Cy3 and Cy5 photobleaching during imaging. Under this imaging condition, only a minor fraction of the time traces were affected by Cy3 or Cy5 photobleaching or photoblinking during the first few minutes of imaging. Despite this precaution, long-lived binding events are influenced by photobleaching, which results in an underestimation of the lifetime of long-lived binding events.

Fluorescence signals from single molecules were collected with a 60× water immersion objective (UPlanSApo, Olympus) with an inverted microscope (IX71, Olympus). Scattering of the 532 nm laser beam was blocked with a 550 nm long-pass filter (LP03–532RU-25, SemRock). When the 633 nm laser was used, 633 nm laser scattering was blocked with a notch filter (NF03–633E-25, SemRock). Subsequently, the signals from Cy3 and Cy5 were spectrally split with a dichroic mirror (λcutoff = 645 nm, Chroma) and imaged onto two halves of an electron multiplying charge-coupled device (EM-CCD) camera (iXon 897, Andor Technology). A series of EM-CCD images were acquired with in-house software written in Visual C++ with a time resolution of 0.3 s. The EM-CCD images record binding events over 25 × 50 μm field of view.

Single-molecule data analysis

Fluorescence images and time traces were extracted with programs written in IDL (ITT Visual Information Solutions) and analyzed with Matlab (MathWorks) and Origin (OriginLab Corporation). To systematically select single molecule fluorescence signals of Cy3 and Cy5 from the acquired images, we employed an algorithm written in IDL that identified fluorescence spots with a defined Gaussian profile and with signals above a threshold. This algorithm was effective in differentiating specific bindings from the background fluorescence.

A dwell-time distribution was fitted by either a single-exponential decay curve ($Ae^{-t/\Delta\tau}$) or a double-exponential decay curve ($A_1e^{-t/\Delta\tau_{short}} + A_2e^{-t/\Delta\tau_{long}}$). In case of a double-exponential decay, the percentages of $\Delta\tau_{short}$ and $\Delta\tau_{long}$ populations are determined by $A_1\Delta\tau_{short}/(A_1\Delta\tau_{short} + A_2\Delta\tau_{long})$ and $A_2\tau_{long}/(A_1\Delta\tau_{short} + A_2\Delta\tau_{long})$, and the average dwell-time is determined by $(A_1\Delta\tau^2_{short} + A_2\tau^2_{long})/(A_1\Delta\tau_{short} + A_2\Delta\tau_{long})$. t (time) is a variable; and A, A_1, A_2 (amplitudes) and $\Delta\tau$, $\Delta\tau_{short}$, $\Delta\tau_{long}$ (life times) are parameters.

RESULTS

Single-molecule assay for investigating Dcr-2 antagonism by VSRs

To reveal how VSRs repress the RNAi machinery, we developed a single-molecule fluorescence assay and assessed in real-time the interactions between RNAi effectors, viral proteins, and RNAs mimicking cellular and viral RNA species. We focused on understanding how viral proteins interfere with the recognition of dsRNAs by *Drosophila* Dcr-2 and its cofactor LqPD. This assay required the assembly of nucleoprotein complexes (Dcr-2, LqPD, VSRs, and dsRNA molecules) at the single-molecule level.

We prepared biotinylated Dcr-2 protein for surface immobilization. Briefly, Dcr-2 was appended with a short tag called AP (Acceptor Peptide), which was used for biotinylation during protein expression (Figure 1A). Dcr-2 was ectopically expressed in Sf9 insect cells together with the BirA enzyme that biotinylates the AP tag (30–31,35). We tested the efficiency of the *in vivo* biotinylation by incubating AP-Dcr-2 protein with NeutrAvidin and running a western blot analysis. Nearly 100% of AP-Dcr-2 was shifted to higher molecular weight indicating efficient biotinylation (Figure 1B). A cleavage assay confirmed that the biotinylated Dcr-2 was catalytically active in processing a blunt end dsRNA (Figure 1C).

We immobilized the biotinylated Dcr-2 on the surface of a microfluidic chamber using biotin–NeutrAvidin interactions (Figure 1D). We washed away the unbound Dcr-2 proteins and introduced recombinant LqPD into the imaging chamber and incubated for 5 min to promote protein–protein interaction. We flushed out the unbound LqPD pro-

teins and introduced dye-labeled dsRNA. We used total internal reflection fluorescence (TIRF) microscopy to observe the interactions between surface-immobilized Dcr-2–LqPD and dye-labeled dsRNA while excluding the background signal from the freely diffusing dsRNA molecules (Figure 1D and E right most).

When Dcr-2 alone was tested, a low number of dsRNA docking events were recorded (Figure 1E). Only when Dcr-2 was associated with the cofactor LqPD, we observed a large number of binding events, as reflected by the increase of black dots in the EM-CCD image (Figure 1E). This observation shows that LqPD increases the binding affinity of Dcr-2 for dsRNA. When the dye-labeled dsRNA was introduced into a surface that was not treated with Dcr-2 and LqPD, no binding events were observed. This excluded the possibility of non-specific interactions between the RNA and the surface (Figure 1E). LqPD itself has dsRNA binding domains that may mediate the binding when non-specifically absorbed to the surface. To rule out this possibility, we pre-treated the microfluidic chamber with LqPD in the absence of Dcr-2 and then introduced dsRNA. We did not observe significant numbers of binding events, excluding the possibility of non-specific interaction between non-biotinylated LqPD proteins and the imaging surface (Figure 1E). These data show that the binding reported here was mediated by a specific recognition of dsRNA molecules by the Dcr-2–LqPD complex.

We sought to understand how Dcr-2–LqPD binds dsRNA substrates by measuring the kinetics of binding in a pre-steady state condition. We introduced dye-labeled dsRNA into a microfluidic chamber (Figure 1F) and imaged the interactions in real-time. dsRNA docking to a single Dcr-2–LqPD complex is reflected by the sudden appearance of the fluorescence signal as shown in the time traces (Figure 1F). To determine the lifetime of binding, we measured the dwell-time ($\Delta\tau$) from 1649 binding events. Dwell-time analysis revealed that the distribution follows a single-exponential decay with $<\Delta\tau> = 12.5 \pm 2.2$ s that reflects the interaction lifetime between the Dcr-2–LqPD complex and the dsRNA substrate (Figure 1G).

Viral proteins antagonize Dcr-2 by shielding viral RNA molecules

Viral proteins can antagonize the RNAi machinery at different levels. We were particularly interested in RNA binding VSRs from *Drosophila* viruses and chose to study the VP3 protein of DXV (genus *Entomobirnavirus*, family *Birnaviridae*) and the 1A protein of DCV (genus *Cripavirus*, family *Dicistroviridae*). In addition, we included in our analyses the VP3 protein of CYV, a virus originally isolated from wild-caught *Culex pipiens* mosquitoes and, like DXV, a member of the genus *Entomobirnavirus*. As expected from their evolutionary relationship, the CYV and DXV VP3 proteins share extensive sequence homology (Supplementary Figure S5). We took advantage of our single-molecule assay to assess how these viral proteins suppress the recognition of RNA substrates by the endonuclease Dcr-2.

First, we hypothesized that viral proteins might physically interact with the Dcr-2–LqPD complex, thereby preventing the recognition of dsRNA molecules. To test this hypothesis, we pre-incubated Dcr-2–LqPD with the viral proteins within the imaging chamber, promoting protein–protein interaction (Figure 2A). After 5 min incubation, we washed away unbound VSRs and quantified binding of Cy5-labeled 70-nt dsRNA to surface-immobilized Dcr-2–LqPD. Compared to the control condition (Maltose Binding Protein, MBP), none of the VSRs significantly inhibited dsRNA binding activity of Dcr-2–LqPD (Figure 2B and C). This experiment thus revealed the absence of inhibitory protein–protein interaction. It should, however, be noted that this absence of inhibition does not rule out a possibility of direct physical interactions between these VSRs and the Dcr-2–LqPD complex.

Next, we probed whether VSRs might directly bind to dsRNA molecules and prevent the recognition by Dcr-2–LqPD. To test this hypothesis, we pre-incubated dsRNA with VSRs, promoting the assembly of the nucleoprotein complexes (Figure 2D). After 5 min pre-incubation, we flushed them into the imaging chambers containing surface-immobilized Dcr-2–LqPD. As evident from the docked dsRNA molecules in the EM-CCD images (Figure 2E), the viral proteins CYV-VP3, DXV-VP3 and DCV-1A inhibited the dsRNA binding capacity of Dcr-2–LqPD in a dose-dependent manner (Figure 2F). Notably, CYV-VP3 exhibited the highest suppressive activity among the three viral proteins. Eighty percent of the binding events were eliminated at a low concentration of the CYV-VP3 protein (1 nM), whereas an ∼100-fold higher concentration (100 nM) of DXV-VP3 and DCV-1A was required to reach the same efficiency. This distinct suppression efficiency is possibly due to a higher dsRNA binding affinity of CYV-VP3.

Viral proteins bind irreversibly to long dsRNA molecules

The data in Figure 2 suggest that the viral proteins CYV-VP3, DXV-VP3 and DCV-1A inhibit the recognition of dsRNA by Dcr-2–LqPD mainly by physical association with dsRNA. We used single-molecule fluorescence for real-time observations of the physical interaction between viral proteins and dsRNA molecules. CYV-VP3, DXV-VP3, and DCV-1A were expressed as fusion proteins with the MBP tag, which offers the possibility of surface immobilization using biotinylated anti-MBP antibody without constraining functional protein domains (Figure 3A). First, we aimed to visualize the physical interaction between the three VSRs and dsRNA and compare their dsRNA binding affinity. Surface-immobilized VSRs were incubated with 70-nt, fully base-paired dsRNA (Supplementary Figure S1) that mimics viral dsRNA. After 5 min incubation, we washed away the unbound RNA and recorded the binding events by taking EM-CCD snapshots (Figure 3B). All three VSRs showed stable physical interaction with 70-nt dsRNA. Quantification of the binding events revealed that CYV-VP3 has the highest dsRNA-binding activity among the three VSRs proteins (Figure 3C), which is in agreement with the suppression of Dcr-2 recognition data in Figure 2D–F.

Next, we sought to visualize the interaction between VSRs and dsRNA in real-time and uncover binding kinetics by taking advantage of our single-molecule assay and the fast camera. Upon the introduction of 100 pM Cy5-

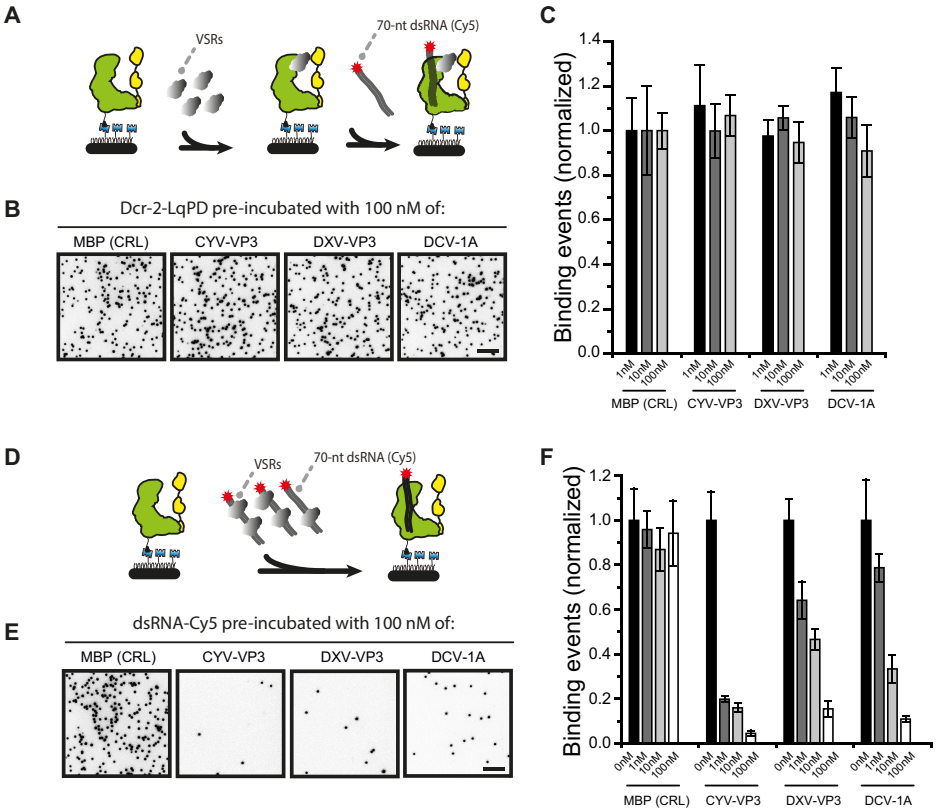

Figure 2. Physical interactions between VSRs and dsRNA inhibit Dcr-2 recognition. (**A**) Schematic representation of single-molecule assay to probe for a direct interaction between the Dcr-2–LqPD complex and VSRs. VSRs were pre-incubated for 5 min with surface immobilized Dcr-2–LqPD to promote protein complex assembly before the introduction of Cy5-labeled 70-nt dsRNA into the imaging chamber. (**B**) EM-CCD images illustrating stable docking of 70-nt Cy5-dsRNA to surface immobilized Dcr-2–LqPD incubated with 100 μM MBP (control, CRL), CYV-VP3, DXV-VP3 or DCV-1A. Scale bar, 5 μm. (**C**) Quantification of dsRNA binding activity of Dcr-2–LqPD complexes that were pre-incubated with the indicated concentration of MBP (reference), CYV-VP3, DXV-VP3 or DCV-1A. The binding events were normalized to the control condition (MBP). Data are presented as averages and SD of three independent experiments. In each experiment snapshots from 10 fields of view were analyzed. (**D**) Schematic of single-molecule assay to probe for an inhibitory interaction between VSRs and Cy5 labeled 70-nt dsRNA. VSRs were incubated with dsRNA for 5 min to promote the assembly of nucleoprotein complexes. After incubation, the nucleoprotein complexes were introduced into the imaging chamber to assess the dsRNA-binding activity of Dcr-2–LqPD. (**E**) EM-CCD images illustrating dsRNA binding activity of surface-immobilized Dcr-2–LqPD to a dsRNA pre-incubated with 100 nM of MBP (control, CRL), CYV-VP3, DXV-VP3 or DCV-1A. Scale bar, 5 μm. (**F**) Quantification of RNA binding activity of Dcr-2–LqPD to dsRNA pre-incubated with different concentrations of MBP, CYV-VP3, DXV-VP3 or DCV-1A. The binding events were normalized to the control condition in which the dsRNA were incubated with the imaging buffer without proteins. Data are presented as averages and SD of three independent experiments. In each experiment snapshots from 10 fields of view were analyzed.

labeled 70-nt dsRNA into an imaging chamber, the encounter with surface-immobilized VSRs was recorded as a sudden appearance of the fluorescence signal. The analysis of time traces exhibited two distinct binding events (Figure 3D, F and H). The short binding reflects an aborted interaction, whereas long binding events indicate a stable (nearly irreversible) interaction between dsRNA and surface-immobilized viral proteins. A substantial number of time traces exhibited very long binding that went beyond the time window of our measurements. To estimate the lifetime of interactions, we built a dwell-time histogram from several hundreds of binding events recorded during the first 7.5 min after introducing dsRNA.

For the CYV-VP3 protein, the data distribution showed a pattern characteristic of photobleaching, with a significant population of dsRNA that survived the imaging (the last bin in the histogram). Our analysis suggested that the majority of binding events were long-lived and the average lifetime of binding under this experimental condition was 151.3 ± 7.4 s (Figure 3E). To estimate the lifetime of the interaction between CYV-VP3 and dsRNA while minimizing the influence of the photobleaching, we took snapshots of fields of view every 2 min and counted the survival of binding events over time. The half-life of the interactions exceeded 70 min (Supplementary Figure S2a).

We performed similar measurements using DXV-VP3 (Figure 3F) and DCV-1A (Figure 3H) and observed a different behavior of dsRNA binding. The binding dwell-time of DXV-VP3 was fitted with a double exponential decay function that reflects two distinct binding modes: a short-lived binding ($\Delta\tau_1 = 8.8 \pm 2.8$ s) and a stable binding ($\Delta\tau_2 = 91.8 \pm 17.9$ s) (Figure 3G), and time traces showed that a single protein can exhibit both short and long binding behavior (Figure 3F). DCV-1A protein also exhibited two distinct binding behaviors, short with $\Delta\tau_1 = 4.9 \pm 2.1$ s life-time and long with $\Delta\tau_2 = 64.0 \pm 16.5$ s life-time (Figure 3H and I). The snapshot measurement further indicated that the half-life of the stable bindings exceed 50 and 34 min

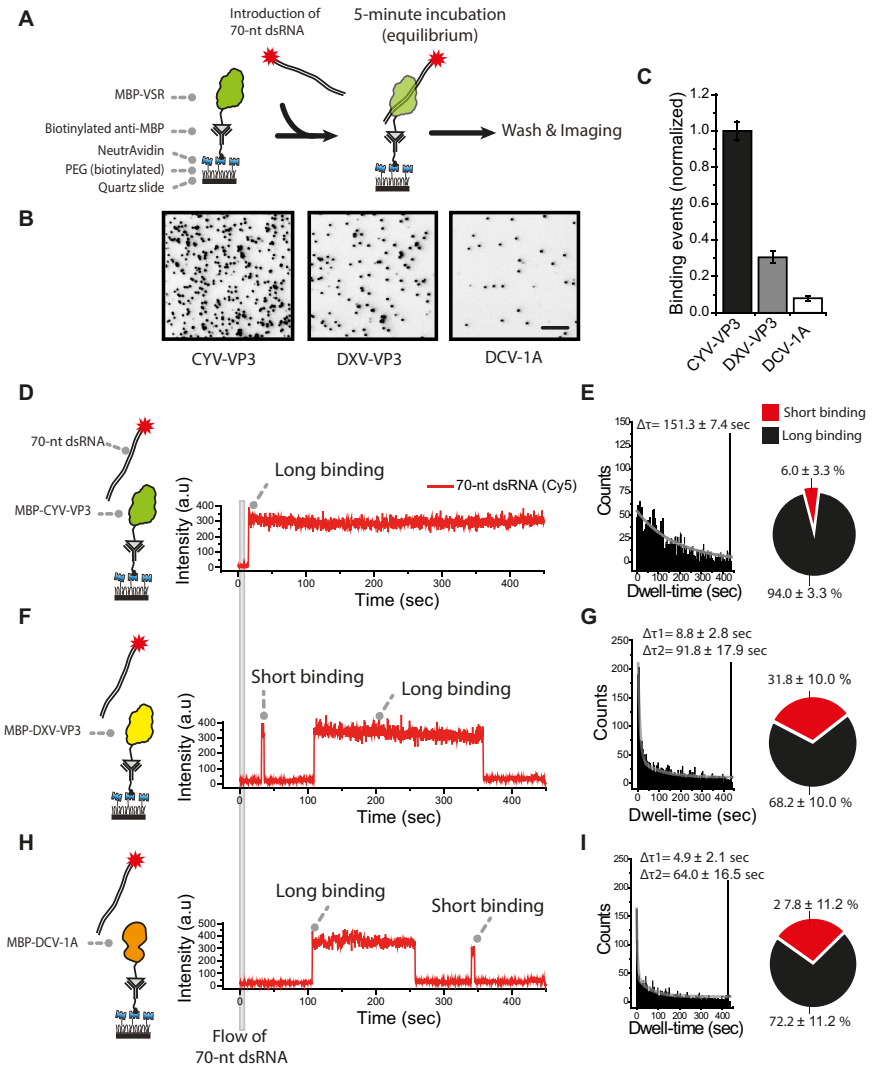

Figure 3. VSRs stably bind to long dsRNA molecules. (**A**) Schematic representation of single-molecule assay to visualize dsRNA recognition by VSRs in steady state conditions. Biotinylated Anti-MBP antibody was conjugated to a polymer-coated surface via NeutrAvidin–biotin interaction. VSRs were incubated for 5 min with the surface-immobilized anti-MBP to promote the interaction on the surface of the imaging chamber. Non-bound VSRs were washed away before Cy5-labeled 70-nt dsRNA was introduced. VSRs and dsRNA were incubated in the imaging for 5 min to reach equilibrium. The unbound dsRNA molecules were washed away before imaging. (**B**) EM-CCD images illustrating dsRNA binding activity of surface-immobilized (50 nM) CYV-VP3, DXV-VP3 and DCV-1A at steady state conditions. Scale bar, 5 μm. (**C**) Quantification of dsRNA binding activity of surface-immobilized CYV-VP3, DXV-VP3 and DCV-1A. Data are normalized and presented as average and SD of three independent experiments. Snapshots from 10 fields of view were analyzed in each experiment. (**D**, **F** and **H**) Representative time traces (at a time resolution of 300 ms) reflecting the recognition of 70-nt dsRNA by CYV-VP3 (D), DXV-VP3 (F) and DCV-1A (H) in pre-steady state conditions. The Cy5-labeled 70-nt dsRNA was introduced in the imaging chamber at $t = 5$ s. (**E**, **G** and **I**) Dwell-time histogram derived from binding events to surface-immobilized CYV-VP3 (E), DXV-VP3 (G) and DCV-1A (I) recorded for 450 s in pre-steady state conditions. The distribution was fitted with a single exponential decay (gray line in E) or double exponential decay (gray line in G and I). Data are presented as average and SD of three independent experiments. The last bin at the end of the histograms represents the binding events that survived beyond 450 s of imagining. The pie charts (right panels) illustrate the percentage of short (red) and long (black) binding events. The cut-off between short and long binding is 10 s.

for DXV-VP3 and DCV-VP3, respectively (Supplementary Figure S2b and c). These data show physical interactions between the viral proteins and dsRNA and demonstrate the higher binding affinity of CYV-VP3 due to the domination of the stable binding.

The length of the RNA stem region defines the binding mode

The intracellular compartment contains a large variation of structured RNAs species. Viral proteins must have a mechanism to specifically distinguish viral from cellular RNA molecules. We sought to find out whether the length of the stem region could affect the recognition by the three VSRs. We used our single-molecule assay to probe VSR binding to a short (22-nt) duplex RNA with two mismatches (Supplementary Figure S1). Time traces revealed an exclusively transient binding behavior for all VSRs tested (Figure 4A, C and E). To accurately estimate the binding dwell-time, we built histograms from several thousands of binding events and noticed that the binding follows a single exponential

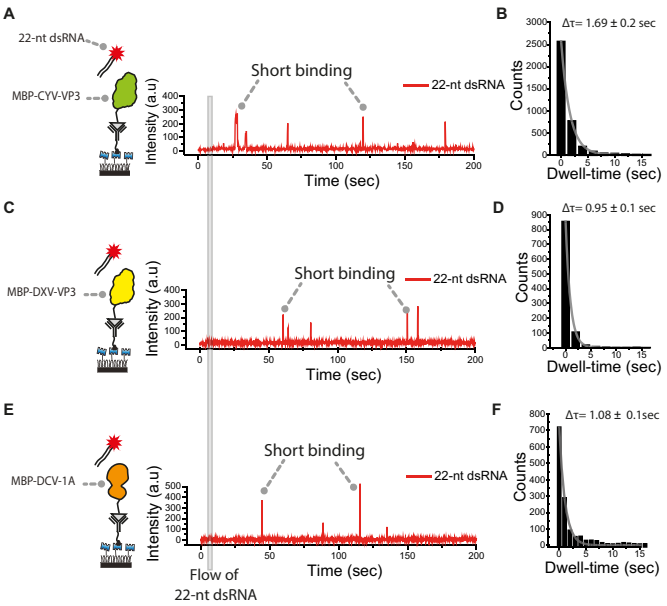

Figure 4. Short RNAs are rapidly rejected by the VSRs after initial sensing. (**A**, **C** and **E**) Representative time traces (at a time resolution of 300 ms) reflecting the recognition of 22-nt dsRNA by CYV-VP3 (A), DXV-VP3 (C) and DCV-1A (E) in pre-steady state conditions. The 22-nt dsRNA contains 2-nt 3′overhang and two mismatches in the base-paired region. The RNA was introduced in the imaging chamber at $t = 5$ s. (**B**, **D** and **F**) Dwell-time histogram derived from binding events to surface-immobilized CYV-VP3 (B), DXV-VP3 (D) and DCV-1A (F) recorded for 450 s in a pre-steady state condition. The distribution was fitted with a single-exponential decay (gray line). Data are presented as average and SD of three independent measurements.

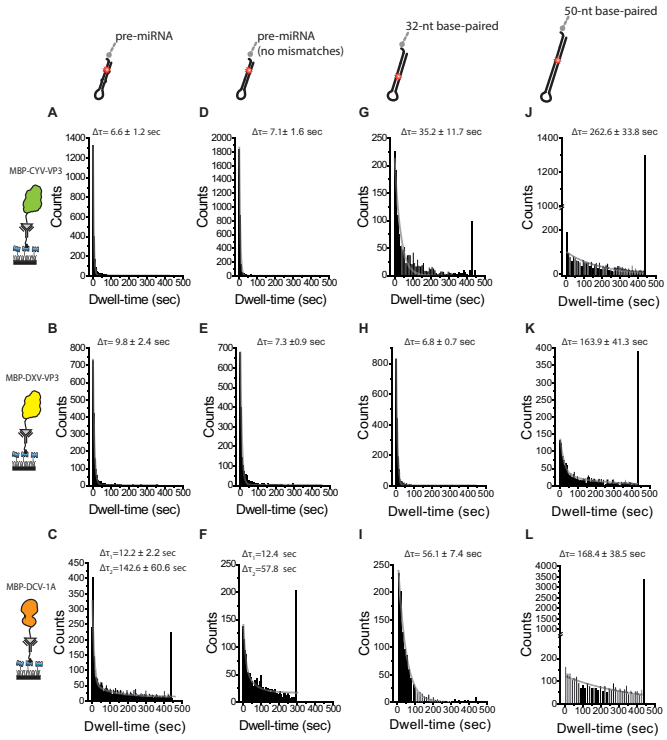

Figure 5. Minimum length of dsRNAs for switching from unstable to stable binding. (**A**–**C**) Dwell-time histograms derived from binding events of pre-miRNA to CYV-VP3 (A), DXV-VP3 (B) and DCV-1A (C) in pre-steady state conditions. The RNA substrate has 20-nt base-paired stem containing two mismatches and 2-nt 3' overhang. (**D**–**F**) Binding dwell-time of pre-miRNA without mismatches in the stem to CYV-VP3 (D), DXV-VP3 (E) and DCV-1A (F) in pre-steady state conditions. The RNA substrate has 20-nt fully base-paired stem and 2-nt 3' overhang. (**G**–**I**) Binding dwell-time of 32-nt dsRNA to CYV-VP3 (G), DXV-VP3 (H) and DCV-1A (I) in pre-steady state conditions. The RNA substrate has 32-nt fully base-paired stem and 2-nt 3' overhang. (**J**–**L**) Binding dwell-time of 50-nt dsRNA to CYV-VP3 (J), DXV-VP3 (K) and DCV-1A (L) in pre-steady state conditions. The RNA substrate has 50-nt fully base-paired stem and 2-nt 3' overhang. The distributions were fitted with either single or double-exponential decay (gray lines). Data are presented as average and SD of three independent measurements.

decay. The binding dwell-time of CYV-VP3, DXV-VP3 and DCV-1A was 1.69 ± 0.2 s, 0.95 ± 0.1 s and 1.08 ± 0.1 s, respectively (Figure 4B, D and F). We observed similar short binding behavior when we tested a short duplex RNA (22-nt) lacking mismatches (Supplementary Figure S3). Such exclusively short interactions might represent a mechanism by which the viral proteins inspect dsRNA molecules and reject non-viral ones.

We sought to define the minimal stem-length required for the VSRs to switch from the rapid rejection to the irreversible binding mode by testing several different dsRNA molecules. First, we tested a precursor microRNA (pre-miRNA) called pre-let-7a-1 that contains a 22-nt base-paired region and a terminal loop (Supplementary Figure S1). We noticed that CYV-VP3 and DXV-VP3 proteins could not stably associate with this pre-miRNA molecule and rejected it within 6.6 ± 1.2 s and 9.8 ± 2.4 s, respectively (Figure 5A and B). In contrast, DCV-1A exhibited a biphasic binding behavior to the pre-miRNA substrate: a population of DCV molecules displayed short binding that reflects an aborted interaction (12.2 ± 2.2 s) and a large population could bind to this substrate stably (142.6 ± 60.6 s) (Figure 5C). The analysis of time traces showed that a single DCV-1A protein can exhibit both short and long binding behavior, excluding the possibility of heterogeneous protein populations (Supplementary Figure S4). These observations suggest a distinct substrate recognition mechanism employed by DCV-1A compared to CYV-VP3 and DXV-VP-3.

Next, we questioned whether the mismatches on the stem region of the pre-miRNA could affect the binding mode. We established a new pre-miRNA construct lacking the mismatches in the stem region and tested the binding mode of the three viral proteins. No difference in binding was observed compared to the pre-let-7a-1 with mismatches, indicating little or no influence of the two mismatches on the stability of the VSR–dsRNA interaction (Figure 5D–F).

Finally, we extended the length of the stem region to 32 base-paired nucleotides and tested the binding behavior of the three viral proteins. The CYV-VP3 shifted its binding mode from unstable to stable when a dsRNA substrate has 32-nt base-paired region ($\Delta\tau = 37.7 \pm 8.0$ s) (Figure 5G). DXV-VP3, however, still exhibited an exclusive rapid rejection mode for this dsRNA substrate ($\Delta\tau = 6.8 \pm 0.7$ s) (Figure 5H). When we tested a dsRNA with a 50-nt stem region, DXV-VP3 like the other two viral proteins shifted to a stable

binding mode (Figure 5J–L). Taken together, these results indicate that DXV-VP3 requires a dsRNA length between 32 and 50-nt to achieve a stable binding, whereas CYV-VP3 requires between 22 and 32-nt dsRNA region to bind stably. DCV-1A was able to stably associate with shorter dsRNA (pre-miRNA) with only 22 basepaired nucleotides and terminal loop, but most stably bound to dsRNA of 50-nt or longer.

DISCUSSION

Antiviral RNAi is a well-conserved defense mechanism that efficiently targets viral RNAs in eukaryotic organisms. In the arms race with their hosts, viruses evolved a multitude of VSR proteins to counteract the antiviral RNAi pathway at different stages (2). The intracellular environment of the host contains a mixture of cellular and viral RNAs, yet VSRs employ a poorly understood mechanism to effectively discriminate viral RNAs from cellular RNAs. We developed sensitive single-molecule assays to gain a dynamic understanding of this discrimination process employed by three VSRs (CYV-VP3, DXV-VP3 and DCV-1A) isolated from different viral species. Of these, DCV-1A contains a canonical dsRNA-binding domain (dsRBD) (11), whereas birnaviral VP3 proteins recognize dsRNA independent of a canonical dsRBD (discussed below) (36). We focused on defining the critical RNA features required for VSR recognition to ensure the protection from Dcr-2 recognition. We found that VSRs employ a rapid screening mechanism and predominantly rely on the length of the double-stranded region to find their targets among a pool of small RNA species that they stochastically encounter. The tested VSRs engage in stable, almost irreversible, binding with RNA species containing long dsRNA motifs (Figure 6).

All tested VSRs efficiently bind dsRNA, which was reflected in the high suppression of viral RNA recognition by Dcr-2 (Figure 2). dsRNA binding to VSRs appears to mask this substrate from Dcr-2 complex recognition. The real-time observations on the recognition process provided direct evidence of physical interactions between VSRs and dsRNA molecules (Figure 3). It also revealed the high RNA-binding activity of these proteins, given that 68–94% of the encounters with the long dsRNA molecules exhibited stable and almost irreversible binding behavior (Figure 3). These observations imply that VSRs can bind long double-stranded RNAs such as the genome of dsRNA viruses and viral replication intermediates of single-stranded RNA viruses with high affinity to mask Dcr-2 recognition. Despite these similarities between the modes of action of these VSRs, they differed in binding efficiency to some RNA species.

CYV and DXV are members of the genus *Entomobirnavirus* (family *Birnaviridae*). VP3 proteins of this family are proposed to mediate capsid assembly through interactions with the viral genome and the RNA-dependent RNA polymerase VP1 (37,38). The carboxy-terminal domain of certain VP3 proteins is highly basic, since it contains dozens of positively charged amino-acids and several proline residues that could mediate the interaction with dsRNAs. Within the birnavirus family, the structure of the dsRNA-binding central domain of VP3 of infectious bursal disease virus (IBDV, genus *Avibirnavirus*) has been solved (36). IBDV VP3 consists of two helical domains connected by a long flexible linker, forming a stable dimer. VP3 sequence homology between entomobirnaviruses and avibirnaviruses is too low to generate a reliable alignment (36), precluding the possibility to generate a homology model for CYV and DXV. Yet, given that birnaviruses share their genome organization and that VP3 of multiple birnavirus genera have been reported to bind dsRNA, it is likely that VP3 of entomobirnaviruses and IBDV share the same common ancestor, and thus to have the same protein fold. It is therefore unexpected that some differences were noted between CYV and DXV VP3 proteins.

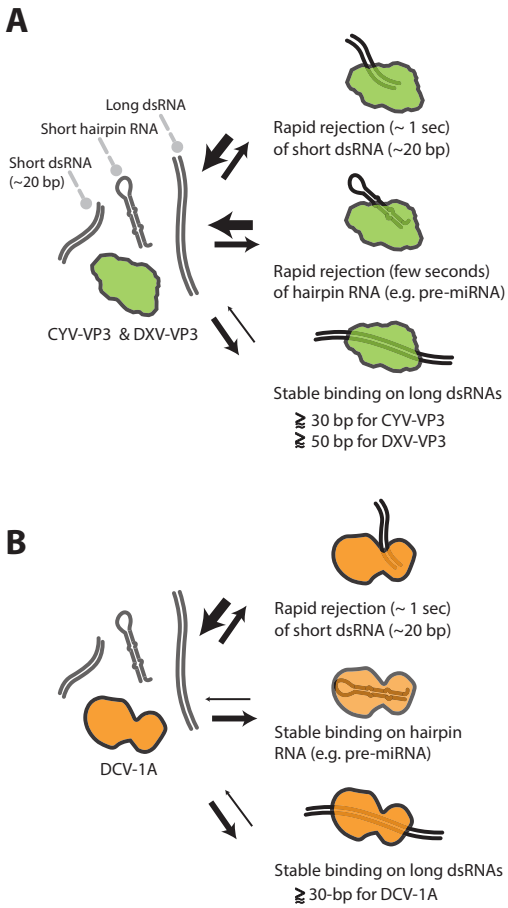

Figure 6. Model of substrate recognition by VRSs. (**A**) CYV-VP3 and DXV-VP3 use a rapid screening mode to discriminate viral dsRNAs from cellular RNAs such as short dsRNAs and short hairpin RNAs. RNAs containing ∼20-bp or shorter ds motif (e.g. duplex miRNAs, vsiRNAs) are rapidly rejected after probing (top). RNAs with a short hairpin structure such as pre-miRNAs are also rapidly rejected (middle). CYV-VP3 and DXV-VP3 stably interact with RNA molecules harboring 30–50 bp or longer ds motif. This stable interaction shields viral RNAs from Dcr-2 recognition and processing (bottom). (**B**) DCV-1A uses a rapid screening mode to discriminate viral dsRNAs from cellular RNAs such as short dsRNAs. RNAs containing ∼20-bp or shorter ds motif are rapidly rejected (top). DCV-1A stably interacts with pre-miRNAs and may affect their maturation into miRNAs (middle). DCV-1A stably interacts with RNA molecules harboring 30 bp or longer ds motifs. These stable interactions shield the RNAs from Dcr-2 (bottom).

CYV-VP3 and DXV-VP3 share 51.6% of sequence identity and 83% of sequence homology at the amino acid level (Supplementary Figure S5). Both proteins were reported to suppress the RNAi pathway *in vivo* (20), and our data indicate that both proteins stably bind long dsRNA, but were not able to stably associate with dsRNA molecules shorter than ∼2-nt and rejected these non-canonical substrates rapidly after few seconds of sensing. We found that despite the sequence homology, the two VSR employ different dynamics when sensing dsRNA molecules. First, DXV-VP3 exhibits a lower dsRNA-binding activity toward the long dsRNA compared to CYV-VP3 (Figure 3A–C). The lower binding activity of DXV-VP3 was also reflected by 31.8% of aborted binding events after the initial interactions, whereas CYV-VP3 failed in engaging stable binding in only 6% of tentative binding (Figure 3D–G). Second, DXV-VP3 protein requires dsRNA region longer than 32-nt to achieve stable binding, whereas the minimal length for CYV-VP3 binding is between 22 and 32 bp of dsRNA (Figure 5). The structural basis for the dsRNA binding activities and the differences between DXV and CYV remain to be determined. Perhaps more importantly, it remains an open question whether the differences in length requirements and affinity reflect different evolutionary pressures in the host species of these viruses.

The aborted interactions with short RNA species suggest that both CYY-VP3 and DXV-VP3 are unlikely to interfere with loading of duplex vsiRNAs into Argonaute via direct binding to duplex RNAs (Figure 4 and Supplementary Figure S4). They briefly interacted with these RNA molecules and rejected them after a few seconds of probing. These results are somewhat contradictory with previous functional and gel-shift assays in which it was proposed that DXV-VP3 and CYV-VP3 have the potential to bind siRNAs (albeit with 30- to 40-fold lower affinity than long dsRNA). Of note, the concentrations of VSRs used in single-molecule analyses are in the range of 100 pM, more than four orders of magnitude lower than the concentrations that showed bindings in the gel-shift assay (K_d 2–6 μM), which may explain the discrepancy between these assays. Additionally or alternatively, in these single-molecule experiments, the VSRs have been immobilized on the glass slide, whereas gel-shift assays are in solution, perhaps favoring higher-order interactions, such as oligomerizations (39), which may contribute to RNA binding.

DCV-1A exhibited one order of magnitude lower binding affinity for long dsRNA than CYV-VP3 (Figure 3). This was evident from the observation that 27.8% of the DCV-1A-dsRNA encounters failed in achieving protective binding. It would be of interest to correlate structural information with binding dynamics to explain why certain RNA-interacting proteins exhibit high binding affinity compared to others. DCV-1A exhibited a notable capability to bind dsRNAs species that are relatively short such as pre-miRNAs with terminal loop and 22-nt basepaired stem region. Based on this result, we anticipate that unlike CYV and DXV infection, DCV infection might deregulate miRNAs biogenesis of the insect host, since the DCV-1A may sequester some of the pre-miRNAs species. Although DCV was suggested not to affect miR-2b biogenesis or function (11), a recent report demonstrated that the levels of a large number of mature miRNAs are reduced upon infection of adult flies, whereas it had not been studied whether this is due to the activity of DCV-1A (40).

Viruses replicate their genomes in dedicated compartments in the cell. For examples, positive-sense RNA viruses remodel intracellular organelles to form so-called replication organelles (41). These structures contain viral genomes and proteins, together with cellular biomolecules that are required for RNA replication. Such viral organelles might offer a local environment that fosters stochastic encounters between VSRs and viral RNAs *in vivo*. It would be of great interest to test our substrate recognition model using *in vivo* approaches such as VSR pulldown combined with RNA-sequencing or single-molecule imaging in living insects or insect cells infected with viruses.

Taken together, our data contribute to the understanding of the molecular basis governing the recognition and protection of viral RNAs by VSRs. However, it remains unclear how RNA-interacting proteins that are beneficial for the viruses (e.g. replication and translation machineries) can dynamically access viral genomes and replication intermediates despite the protection by VSRs. Real-time observations of the interplay between viral dsRNA, VSRs, and other RNA-interacting proteins may shed light on this intriguing problem.

DATA AVAILABILITY

The data and the computer codes that support the findings of this study are available from the authors on request.

SUPPLEMENTARY DATA

Supplementary Data are available at NAR Online.

ACKNOWLEDGEMENTS

We thank members of the Van Rij and Joo laboratories for the technical help and insightful discussions. We thank John Strouboulis (B.S.R.C. Alexander Fleming) for sharing the BirA plasmid.

Author Contributions: M.F., R.v.R. and C.J. designed the research; M.F. performed the single-molecule experiments with helps from I.K. and J.V.L.; M.F., A.C.H. and A.W.B. performed proteins purification and bulk experiments; M.F., I.K. and J.V.L. analyzed the data; M.F., I.K., J.V.L., A.C.H., R.V.R and C.J. discussed the data; M.F., R.V.R. and C.J. wrote the manuscript.

FUNDING

Netherlands Organization for Scientific Research [Vidi grant 864.14.002 to C.J.]; European Research Council Starting Grant under the European Union's Seventh Framework Programme [FP7/2007–2013/ERC grant 309509 to C.J.]; European Research Council Consolidator Grant under the European Union's Seventh Framework Programme [FP7/2007–2013/ERC grant 615680 to R.v.R.]; Fondation pour la Recherche Medicale [SPE20120523964 to M.F.]. Funding for open access charge: Netherlands Organization for Scientific Research [Vidi grant 864.14.002 to C.J.].

Conflict of interest statement. None declared.

REFERENCES

1. Obbard,D.J., Gordon,K.H., Buck,A.H. and Jiggins,F.M. (2009) The evolution of RNAi as a defence against viruses and transposable elements. *Philos. Trans. R. Soc. Lond. B Biol. Sci.*, **364**, 99–115.
2. Bronkhorst,A.W. and van Rij,R.P. (2014) The long and short of antiviral defense: small RNA-based immunity in insects. *Curr. Opin. virol.*, **7**, 19–28.
3. Aguiar,E.R., Olmo,R.P. and Marques,J.T. (2016) Virus-derived small RNAs: molecular footprints of host-pathogen interactions. *Wiley Interdiscip. Rev. RNA*, **7**, 824–837.
4. Olson,K.E. and Blair,C.D. (2015) Arbovirus-mosquito interactions: RNAi pathway. *Curr. Opin. Virol.*, **15**, 119–126.
5. Sinha,N.K., Trettin,K.D., Aruscavage,P.J. and Bass,B.L. (2015) Drosophila dicer-2 cleavage is mediated by helicase- and dsRNA termini-dependent states that are modulated by Loquacious-PD. *Mol. Cell*, **58**, 406–417.
6. Sinha,N.K., Iwasa,J., Shen,P.S. and Bass,B.L. (2017) Dicer uses distinct modules for recognizing dsRNA termini. *Science*, eaaq0921.
7. Schirle,N.T. and MacRae,I.J. (2012) The crystal structure of human Argonaute2. *Science*, **336**, 1037–1040.
8. Schirle,N.T., Sheu-Gruttadauria,J. and MacRae,I.J. (2014) Structural basis for microRNA targeting. *Science*, **346**, 608–613.
9. Lingel,A., Simon,B., Izaurralde,E. and Sattler,M. (2003) Structure and nucleic-acid binding of the Drosophila Argonaute 2 PAZ domain. *Nature*, **426**, 465–469.
10. Mueller,S., Gausson,V., Vodovar,N., Deddouche,S., Troxler,L., Perot,J., Pfeffer,S., Hoffmann,J.A., Saleh,M.C. and Imler,J.L. (2010) RNAi-mediated immunity provides strong protection against the negative-strand RNA vesicular stomatitis virus in Drosophila. *Proc. Natl. Acad. Sci. U.S.A.*, **107**, 19390–19395.
11. van Rij,R.P., Saleh,M.C., Berry,B., Foo,C., Houk,A., Antoniewski,C. and Andino,R. (2006) The RNA silencing endonuclease Argonaute 2 mediates specific antiviral immunity in Drosophila melanogaster. *Genes Dev.*, **20**, 2985–2995.
12. Galiana-Arnoux,D., Dostert,C., Schneemann,A., Hoffmann,J.A. and Imler,J.L. (2006) Essential function in vivo for Dicer-2 in host defense against RNA viruses in drosophila. *Nat. Immunol.*, **7**, 590–597.
13. Marques,J.T., Wang,J.P., Wang,X., de Oliveira,K.P., Gao,C., Aguiar,E.R., Jafari,N. and Carthew,R.W. (2013) Functional specialization of the small interfering RNA pathway in response to virus infection. *PLoS Pathogens*, **9**, e1003579.
14. Li,H., Li,W.X. and Ding,S.W. (2002) Induction and suppression of RNA silencing by an animal virus. *Science*, **296**, 1319–1321.
15. Wang,X.H., Aliyari,R., Li,W.X., Li,H.W., Kim,K., Carthew,R., Atkinson,P. and Ding,S.W. (2006) RNA interference directs innate immunity against viruses in adult Drosophila. *Science*, **312**, 452–454.
16. Nayak,A., Berry,B., Tassetto,M., Kunitomi,M., Acevedo,A., Deng,C., Krutchinsky,A., Gross,J., Antoniewski,C. and Andino,R. (2010) Cricket paralysis virus antagonizes Argonaute 2 to modulate antiviral defense in Drosophila. *Nat. Struct. Mol. Biol.*, **17**, 547–554.
17. Sullivan,C.S. and Ganem,D. (2005) A virus-encoded inhibitor that blocks RNA interference in mammalian cells. *J. Virol.*, **79**, 7371–7379.
18. Bronkhorst,A.W., van Cleef,K.W., Vodovar,N., Ince,I.A., Blanc,H., Vlak,J.M., Saleh,M.C. and van Rij,R.P. (2012) The DNA virus Invertebrate iridescent virus 6 is a target of the Drosophila RNAi machinery. *Proc. Natl. Acad. Sci. U.S.A.*, **109**, E3604–E3613.
19. Aliyari,R., Wu,Q., Li,H.W., Wang,X.H., Li,F., Green,L.D., Han,C.S., Li,W.X. and Ding,S.W. (2008) Mechanism of induction and suppression of antiviral immunity directed by virus-derived small RNAs in Drosophila. *Cell Host Microbe*, **4**, 387–397.
20. van Cleef,K.W., van Mierlo,J.T., Miesen,P., Overheul,G.J., Fros,J.J., Schuster,S., Marklewitz,M., Pijlman,G.P., Junglen,S. and van Rij,R.P. (2014) Mosquito and Drosophila entomobirnaviruses suppress dsRNA- and siRNA-induced RNAi. *Nucleic Acids Res.*, **42**, 8732–8744.
21. Lu,R., Maduro,M., Li,F., Li,H.W., Broitman-Maduro,G., Li,W.X. and Ding,S.W. (2005) Animal virus replication and RNAi-mediated antiviral silencing in Caenorhabditis elegans. *Nature*, **436**, 1040–1043.
22. Singh,G., Popli,S., Hari,Y., Malhotra,P., Mukherjee,S. and Bhatnagar,R.K. (2009) Suppression of RNA silencing by Flock house virus B2 protein is mediated through its interaction with the PAZ domain of Dicer. *FASEB J.*, **23**, 1845–1857.
23. van Mierlo,J.T., Bronkhorst,A.W., Overheul,G.J., Sadanandan,S.A., Ekstrom,J.O., Heestermans,M., Hultmark,D., Antoniewski,C. and van Rij,R.P. (2012) Convergent evolution of argonaute-2 slicer antagonism in two distinct insect RNA viruses. *PLoS Pathogens*, **8**, e1002872.
24. van Mierlo,J.T., Overheul,G.J., Obadia,B., van Cleef,K.W., Webster,C.L., Saleh,M.C., Obbard,D.J. and van Rij,R.P. (2014) Novel Drosophila viruses encode host-specific suppressors of RNAi. *PLoS Pathogens*, **10**, e1004256.
25. Juette,M.F., Terry,D.S., Wasserman,M.R., Zhou,Z., Altman,R.B., Zheng,Q. and Blanchard,S.C. (2014) The bright future of single-molecule fluorescence imaging. *Curr. Opin. Chem. Biol.*, **20**, 103–111.
26. Joo,C., Fareh,M. and Kim,V.N. (2013) Bringing single-molecule spectroscopy to macromolecular protein complexes. *Trends Biochem. Sci*, **38**, 30–37.
27. van Oijen,A.M. (2011) Single-molecule approaches to characterizing kinetics of biomolecular interactions. *Curr. Opin. Biotechnol.*, **22**, 75–80.
28. Hoskins,A.A., Friedman,L.J., Gallagher,S.S., Crawford,D.J., Anderson,E.G., Wombacher,R., Ramirez,N., Cornish,V.W., Gelles,J. and Moore,M.J. (2011) Ordered and dynamic assembly of single spliceosomes. *Science*, **331**, 1289–1295.
29. Ye,X. and Liu,Q. (2008) Expression, purification, and analysis of recombinant Drosophila Dicer-1 and Dicer-2 enzymes. *Methods Mol. Biol.*, **442**, 11–27.
30. Fareh,M., Loeff,L., Szczepaniak,M., Haagsma,A.C., Yeom,K.H. and Joo,C. (2016) Single-molecule pull-down for investigating protein-nucleic acid interactions. *Methods*, **105**, 99–108.
31. Fareh,M., Yeom,K.H., Haagsma,A.C., Chauhan,S., Heo,I. and Joo,C. (2016) TRBP ensures efficient Dicer processing of precursor microRNA in RNA-crowded environments. *Nat. Commun.*, **7**, 13694.
32. Stark,M.R., Pleiss,J.A., Deras,M., Scaringe,S.A. and Rader,S.D. (2006) An RNA ligase-mediated method for the efficient creation of large, synthetic RNAs. *RNA*, **12**, 2014–2019.
33. Selvin,P.R. and Ha,T. (2007) *Single-Molecule Techniques: a Laboratory Manual*. 1st edn, Cold Spring Harbor Laboratory Press, New York, USA.
34. Rasnik,I., McKinney,S.A. and Ha,T. (2006) Nonblinking and long-lasting single-molecule fluorescence imaging. *Nat. Methods*, **3**, 891–893.
35. Howarth,M. and Ting,A.Y. (2008) Imaging proteins in live mammalian cells with biotin ligase and monovalent streptavidin. *Nat. Protoc.*, **3**, 534–545.
36. Casanas,A., Navarro,A., Ferrer-Orta,C., Gonzalez,D., Rodriguez,J.F. and Verdaguer,N. (2008) Structural insights into the multifunctional protein VP3 of birnaviruses. *Structure*, **16**, 29–37.
37. Lombardo,E., Maraver,A., Caston,J.R., Rivera,J., Fernandez-Arias,A., Serrano,A., Carrascosa,J.L. and Rodriguez,J.F. (1999) VP1, the putative RNA-dependent RNA polymerase of infectious bursal disease virus, forms complexes with the capsid protein VP3, leading to efficient encapsidation into virus-like particles. *J. Virol.*, **73**, 6973–6983.
38. Tacken,M.G., Peeters,B.P., Thomas,A.A., Rottier,P.J. and Boot,H.J. (2002) Infectious bursal disease virus capsid protein VP3 interacts both with VP1, the RNA-dependent RNA polymerase, and with viral double-stranded RNA. *J. Virol.*, **76**, 11301–11311.
39. Maraver,A., Ona,A., Abaitua,F., Gonzalez,D., Clemente,R., Ruiz-Diaz,J.A., Caston,J.R., Pazos,F. and Rodriguez,J.F. (2003) The oligomerization domain of VP3, the scaffolding protein of infectious bursal disease virus, plays a critical role in capsid assembly. *J. Virol.*, **77**, 6438–6449.
40. Monsanto-Hearne,V., Tham,A.L., Wong,Z.S., Asgari,S. and Johnson,K.N. (2017) Drosophila miR-956 suppression modulates Ectoderm-expressed 4 and inhibits viral replication. *Virology*, **502**, 20–27.
41. Belov,G.A. and van Kuppeveld,F.J. (2012) (+)RNA viruses rewire cellular pathways to build replication organelles. *Curr. Opin. Virol.*, **2**, 740–747.